Electronic structure of multiferroic BiFeO₃ by resonant soft x-ray emission spectroscopy

Tohru Higuchi,[*] Yi-Sheng Liu, Peng Yao, Per-Anders Glans, and Jinghua Guo
Advanced Light Source, Lawrence Berkeley National Laboratory, Berkeley, California 94720, USA

Chinglin Chang
Department of Physics, Tamkang University, Tamsui 251, Taiwan, Republic of China

Ziyu Wu
*Beijing Synchrotron Radiation Facility, Institute of High Energy Physics, Chinese Academy of Sciences,
Beijing 100049, People's Republic of China*

Wataru Sakamoto, Naoyuki Itoh, Tetsuo Shimura, and Toshinobu Yogo
EcoTopia Science Institute, Nagoya University, Nagoya 464-8603, Japan

Takeshi Hattori
Department of Applied Physics, Tokyo University of Science, Tokyo 162-8601, Japan

The electronic structure of multiferroic BiFeO₃ has been studied using soft x-ray emission spectroscopy. The fluorescence spectra exhibit that the valence band is mainly composed of O $2p$ state hybridized with Fe $3d$ state. The band gap corresponding to the energy separation between the top of the O $2p$ valence band and the bottom of the Fe $3d$ conduction band is 1.3 eV. The soft x-ray Raman scattering reflects the features due to the charge-transfer transition from O $2p$ valence band to Fe $3d$ conduction band. These findings are similar to the result of electronic structure calculation by density-functional theory within the local spin-density approximation that included the effect of Coulomb repulsion between localized d states.

I. INTRODUCTION

Multiferroic materials, such as BiFeO₃ (BFO) and YMnO₃, have simultaneous antiferromagnetic, ferroelectric, and/or ferroelastic ordering.[1–6] Coupling between the magnetic and ferroelectric order parameters can lead to magnetoelectric effects, in which the magnetization can be tuned by an applied electric field and vice versa. In particular, BiFeO₃ is a suitable candidate for attaining ferroelectric and antiferromagnetic domain couplings at room temperature (RT), owing to its high Curie temperature of 1100 °C and its high Néel temperature of ~370 °C.[2,3] The crystal structure of BiFeO₃ single crystal is a rhombohedrally distorted perovskite structure, which belongs to the space-group $R3C$ with the unit-cell parameters $a=3.96$ Å and $\alpha=89.4°$.[4] In terms of ferroelectricity, the BiFeO₃ single crystal has a spontaneous polarization of 3.5 $\mu C/cm^2$ along the ⟨100⟩ direction and of 6.1 $\mu C/cm^2$ along the ⟨111⟩ direction.[5] The polarization is strongly enhanced in thin-film forms.

A large polarization above ~50 $\mu C/cm^2$ has been observed in high-quality single crystal and thin films fabricated by pulsed laser deposition (PLD) and chemical solution deposition (CSD).[6–10] Furthermore, in recent years, Kim *et al.*[11] have reported that the BiFeO₃ epitaxial film has the highest polarization of 70–80 $\mu C/cm^2$ on SrTiO₃ (001) substrates with SrRuO₃ bottom electrode {11}. Therefore, BiFeO₃ thin film is expected for the application of a high-density ferroelectric random-access memory because of its large polarization and low crystallization temperature. However, a major problem of BiFeO₃ thin film is its low electrical resistivity, which affects the measurement of dielectric/

ferroelectric properties at RT. The low electrical resistivity of BiFeO₃ thin films is attributed to the valence fluctuations of Fe ions (Fe²⁺ or Fe³⁺), creating oxygen vacancies for charge compensation.[12,13] The BiFeO₃ thin film needs the high electrical resistivity in order to obtain good ferroelectricity. Therefore, the formation of solid solutions with other perovskite materials, as well as the substitution of impurity atoms at the Bi and Fe sites, have been attempted by many scientists.[14–18]

In recent years, BiFeO₃ has been refocused in research area of solid-state physics.[1,6,19,20] Neaton *et al.*[19] have studied theoretically the ground-state structural and electronic properties of BiFeO₃ using the density-functional theory (DFT) within the local spin-density approximation (LSDA). In this calculation, a large ferroelectric polarization of 90–100 $\mu C/cm^2$ is predicted, consistent with the large atomic displacements in the ferroelectric phase and with recent experimental reports.[7–10] The electronic structure calculation of BiFeO₃ with the space-group $R3C$ shows an antiferromagnetic insulatinglike nature and hybridization effect between Fe $3d$ and O $2p$ in the valence band.[19] The authors believe that the electrical properties of BiFeO₃ are closely related to the electronic structure. However, the electronic structure of BiFeO₃ has not been clarified experimentally thus far.

In this study, the electronic structure of BiFeO₃ bulk crystal has been measured by x-ray absorption spectroscopy (XAS) and soft x-ray emission spectroscopy (SXES). Although photoemission spectroscopy (PES) has been a powerful method of studying the electronic structure of total density of state (DOS), PES is surface sensitive since the mean-

free path of an electron is very short. Additionally, the PES cannot study the electronic structure of insulating material due to charging up. Therefore, it is difficult to study the electronic structure of $BiFeO_3$ by PES. SXES is related directly to the occupied DOS.[21] SXES detects the electronic structure of the bulk state owing to the long mean-free path of the soft x rays. Furthermore, the partial DOS (PDOS) localized at an atom can be obtained from SXES spectra because SXES has a clear selection rule regarding the angular momentum due to dipole selection. XAS is related directly to the unoccupied DOS.[22] This optical process is a local process because of the localized core state. It is governed by the dipole selection rules so that XAS provides spectra related to the site- and symmetry-selected DOS. In this paper, the authors discuss the origin of the multiferroic behavior of $BiFeO_3$ by comparing it with nonmultiferroic material.

II. EXPERIMENT

$BiFeO_3$ sample was prepared by a solid-state reaction using conventional milling and firing techniques. Bi_2O_3 and Fe_2O_3 powders corresponding to $BiFeO_3$ composition with 0.75 mol % of excess Bi was weighed and thoroughly mixed using stabilized ZrO_2 balls in ethanol. The mixtures were dried, pressed, and sintered at 750 °C for 2 h at an increment of 10 °C/min. In this case, polyvinyl alcohol was used as a binder. The powder compacts were subsequently sintered at 900–1000 °C for 3–10 h at an increment of 10 °C/min. The prepared samples were characterized by x-ray diffraction with $CuK\alpha$ radiation using a monochromator. Details have been reported in Ref. 18.

XAS and SXES spectra were measured at beamline 7.0.1 at the advanced light source (ALS), Lawrence Berkeley National Laboratory, USA. This beamline is equipped with a spherical grating monochromator.[23] The XAS spectra were obtained by recording the fluorescence yield with 0.2 eV resolution and normalized to the photocurrent from a clean gold mesh to correct the intensity fluctuation of the excitation beam, which reflects the bulk state. SXES spectra were recorded using a Nordgren-type grazing-incidence spherical grating spectrometer.[24,25] The incidence angle of the photon beam was 20° to the sample surface in order to reduce the self-absorption effect. The $BiFeO_3$ sample was fractured before measurement. The SXES spectra were normalized by the measurement time and beam current. The SXES spectrometer was set to have resolutions of 0.5 and 0.7 eV for O 1s and Fe 2p core levels, respectively.

III. RESULTS AND DISCUSSION

Figure 1 shows the Fe 2p XAS spectrum of $BiFeO_3$. The spectrum consists of two parts derived from the spin-orbit split of $L_3(2p_{3/2})$ and $L_2(2p_{1/2})$ states. They are further split into the t_{2g} and e_g states due to the octahedral ligand field. The crystal-field splitting (10 Dq) corresponding to the energy separation between t_{2g} and e_g states is 1.4 eV. The spectral shape, peak positions, and 10 Dq of $BiFeO_3$ are similar to those of $La_{1-x}Sr_xFeO_3$, which was theoretically calculated
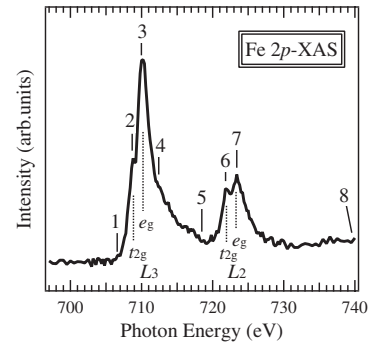

FIG. 1. Fe 2p XAS spectrum of $BiFeO_3$. The labels (1–8) indicate the photon energies where the Fe 2p SXES spectra were measured.

assuming a high-spin $t_{2g}^3 e_g^2$ ground state.[26,27] This fact indicates that the $BiFeO_3$ is mainly $3d^5$ in the ground state of bulk. In recent years, Béa *et al.*[28] have reported the Fe 2p XAS spectra of $BiFeO_3$ thin film. The peak position of this report accords with that of Fig. 1. The intensity ratio $[I(L_2)/I(L_3)]$ of L_3 and L_2 of this report is different from that of Fig. 1. Although the ratio of Fig. 1 is approximately 0.5, the ratio of this report is smaller than 0.5, indicating the effect of surface state. The vertical bars, which are labeled from 1 to 8, indicate the selected photon energies for resonant SXES measurements.

Figure 2 shows the Fe 2p SXES spectra of $BiFeO_3$ excited at photon energies labeled in Fig. 1. It is well known that the Fe 2p emission reflects the Fe 3d PDOS. An arrow shown in each spectrum is attributed to elastic scattering of the excitation photon. The elastic peak is enhanced at the excitation energy corresponding to the e_g absorption peak of
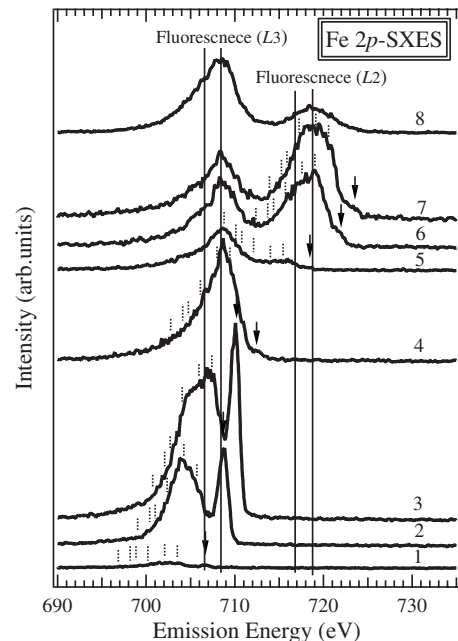

FIG. 2. Fe 2p SXES spectra of $BiFeO_3$ excited at various photon energies indicated in Fig. 1. Arrow shows the energy position of the excitation photon energy. Four vertical solid lines are the energy positions of Fe $3d \rightarrow 2p$ fluorescence.
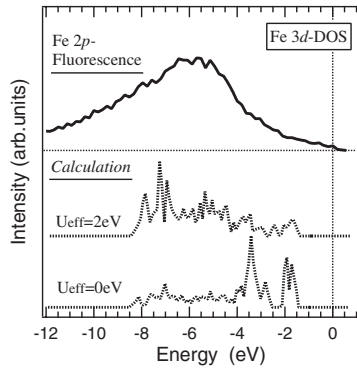
FIG. 3. (a) Fe $2p$ fluorescence spectrum of BiFeO$_3$ and (b) Fe $3d$ PDOS curves calculated by Neaton *et al.* (Ref. 18).

L_3 (spectrum 3 of Fig. 2). The peak intensity decreases with increasing excitation energy for spectra 4 to 7. On the other hand, several features of vertical dashed lines with same energy separations from the excitation energy are attributed to the soft x-ray Raman scattering (or inelastic scattering). The details of soft x-ray Raman scattering will be discussed in Figs. 4 and 5.

The spectrum 8 excited at $h\upsilon = 740$ eV is an off-resonance spectrum attributed to the normal Fe $3d \rightarrow 2p$ fluorescence spectrum. This spectrum may indicate that the Fe $3d$ state hybridizes with O $2p$ state in the valence band. Four solid lines show the fluorescence bands by L_3 and L_2 excitations.

Figure 3 shows the comparison between Fe $2p$ fluorescence spectrum by L_3 excitation and the theoretical Fe $3d$ PDOS calculated by Neaton *et al.*[19,20] Neaton *et al.* calculated the DOS curves using DFT within LSDA.[19] Furthermore, the effect of Coulomb repulsion (U_{eff}) between localized Fe $3d$ states is also included by adding a Hubbard-type term to the effective potential. The Fe $3d$ PDOS at $U_{\text{eff}} = 0$ eV distributes at the top of the valence band. However, the distribution of Fe $3d$ PDOS at $U_{\text{eff}} = 2$ eV shifts to the higher energy side than that at $U_{\text{eff}} = 0$ eV. The distribution of Fe $3d$ PDOS estimated by the Fe $2p$ fluorescence spectrum is similar to that calculated at $U_{\text{eff}} = 2$ eV, although the bandwidth of the calculated DOS is different from that of Fe $2p$ fluorescence spectrum by the effect of energy resolution of this system. The above results indicate that the U_{eff} between localized Fe $3d$ states also plays an important role in the electrical properties of BiFeO$_3$.

Figure 4 shows the SXES spectra of BiFeO$_3$, where the abscissa is the Raman shift (or energy loss) from the elastic scattering. The elastic-scattering peak is located at 0 eV. The Fe $3d \rightarrow 2p$ fluorescence peaks shown by six solid bars shift to the higher energy with increasing excitation energy. Several soft x-ray Raman-scattering peaks shown as vertical dashed lines α, β, χ, δ, ε, and ϕ are observed at 3.2, 4.5, 6.6, 7.8, 8.4, and 9.7 eV, respectively, from the elastic-scattering peak. The soft x-ray Raman-scattering peaks excited at the L_3 absorption edge overlap with the Fe $3d \rightarrow 2p$ fluorescence peaks. The spectrum 1 excited just below the Fe $2p$ threshold shows an apparent feature at a lower energy than the elastic scattering. Since the excitation energy is lower than the binding energy of Fe $2p$ core level, the spectrum 1 is attributed to
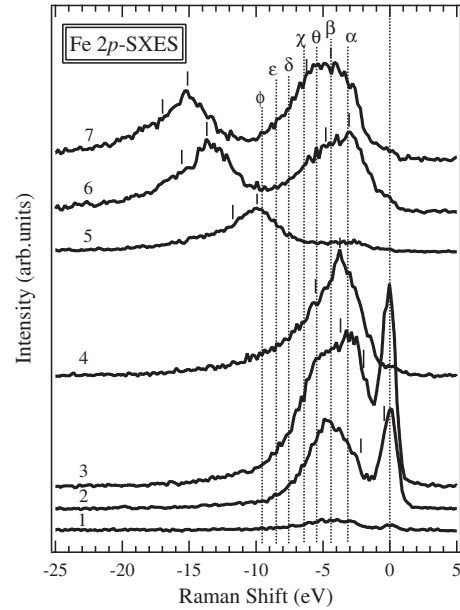

FIG. 4. Fe $2p$ SXES spectra of BiFeO$_3$ presented on a relative emission energy scale compared to the elastic scattering. Vertical dashed lines show the positions of inelastic scattering.

the normal Raman scattering, where the intermediate state is a virtual state. The elementary excitation of the Raman scattering is considered to correspond to the valence-band transition. Therefore, the energy positions of these Raman-scattering peaks may correspond to the transition between the valence and conduction bands.

Figure 5 shows the O $1s$ and Fe $2p$ SXES spectra and O $1s$ XAS spectrum of BiFeO$_3$, where the abscissa is the relative energy to Fermi level (E_F). The O $1s$ and Fe $2p$ SXES spectra were measured at the excitation energies of 540 and 740 eV, respectively. The Fe $2p$ and O $1s$ SXES spectra, which correspond to the fluorescence spectra, reflect
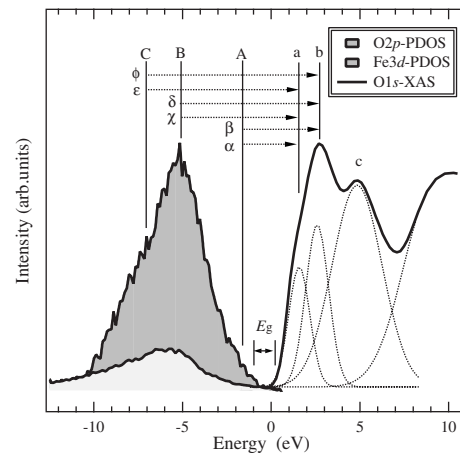

FIG. 5. Fe $2p$ and O $1s$ fluorescence spectra and O $1s$ XAS spectrum of BiFeO$_3$ presented on a relative energy compared to E_F. The energy separation between the top of the valence band and the bottom of conduction band reflects the band gap (E_g) of BiFeO$_3$. Dashed curves are the details of conduction band that were estimated from Gaussian fitting.

the Fe $3d$ and O $2p$ PDOS, respectively, in the valence band. The energy position of O $2p$ state overlaps with that of Fe $3d$ state. This result indicates that the Fe $3d$ state hybridizes with O $2p$ state in the valence band. The O $2p$ valence band has three structures labeled as A, B, and C. The Fe $3d$ contribution is more significant in the B and C peaks, where the O $2p$ states have a larger admixture of Fe $3d$ states. The A peak corresponds to the O $2p$ states, which are not hybridized with the Fe derived states. On the other hand, from the dipole selection rules, it is understood that the O $1s$ XAS spectrum of Fe oxides corresponds to transitions from O $1s$ to O $2p$.[26] The conduction band has three structures shown as dashed curves from Gaussian fitting. The a and b peaks correspond to the t_{2g} and e_g states, respectively, of Fe $3d$ state. The c peak is considered to be Bi $6sp$ state. The energy separation between a and b peaks accords with the result of Fe $2p$ XAS spectrum in Fig. 1. The band gap corresponding to the energy separation between the top of the valence band and the bottom of the conduction band is estimated to be 1.3 eV by concerning the resolution in this measurement system. In LSDA calculation,[19,20] the band gap has been estimated to be 1.3 eV at $U_{\text{eff}}=2$ eV, although the gap is 0.4 eV at $U_{\text{eff}}=0$ eV. The value of $BiFeO_3$ is smaller than those of other ferroelectric material such as $Bi_4Ti_3O_{12}$ and $Pb(Zr,Ti)O_3$ (PZT).[29,30] The small band gap contributes to the low electrical resistivity of $BiFeO_3$ bulk crystal. In recent years, Ihlefeld *et al.*[31] have reported that the epitaxial $BiFeO_3$ thin film on $SrTiO_3$ substrate has the band gap of 2.74 eV. The discrepancy is considered to originate the difference of electron correlation energy between thin film and ceramic sample because the band gap is defined by the energy separation between Fe $3d$ valence and Fe $3d$ conduction bands. The BFO ceramics sample used in this study has valence fluctuations of Fe ions (Fe^{2+} or Fe^{3+}), creating oxygen vacancies for charge compensation as shown in Fig. 1. Thus, the band gap of BFO ceramics sample may decrease due to the decrease in electron correlation energy with oxygen vacancies and valence fluctuations of Fe ions, although the evidence has not been clarified thus far.

Here, the authors estimate the six soft x-ray Raman-scattering peaks (α, β, χ, δ, ε, and ϕ) in Fig. 4. α (β) corresponds to the transitions from A to a (b). χ (δ) corresponds to the transitions from B to a (b). ε (ϕ) corresponds to the transitions from C to a (b). These agreements indicate that the six soft x-ray Raman-scattering peaks are attributed to the charge-transfer (CT) transitions from the occupied O $2p$ to unoccupied Fe $3d$ states. A soft x-ray Raman-scattering peak labeled as θ is strongly observed at $\sim$5.5 eV in Fig. 3.This peak may correspond to the CT transition from the occupied O $2p$ state (B peak) to the bottom of the conduction band, although the evidence has not been clarified

thus far. On the other hand, soft x-ray Raman-scattering peaks due to the d-d transition between the $3d$ valence and conduction bands are observed in SXES spectra of lightly $3d$ transition-metal compounds.[32–37] In particular, the t_{2g} resonant SXES spectra exhibit the Raman scattering due to d-d transition corresponding to the half of electron correlation energy.[34,36] However, the authors cannot estimate such a scattering from the spectra of Fig. 4, although that may exist.

Finally, the authors discuss about the origin of multiferroic behavior of $BiFeO_3$ by comparing it with nonmultiferroic material such as $Bi_4Ti_3O_{12}$ (BIT) and PZT.[29,30] In both BIT and PZT, the valence band consists of O $2p$ state hybridized with Ti $3d$ state and the conduction band consists of Ti $3d$ state. Furthermore, these SXES data exhibit the several soft x-ray Raman-scattering peaks, which attribute to CT transitions. These situations are similar to $BiFeO_3$. The difference between $BiFeO_3$ and BIT (PZT) is the electron number of $3d$ state and origin of band gap. The band gaps of BIT and PZT with $3d^0$ configuration is determined by the energy separation between the top of O $2p$ valence band and the bottom of Ti $3d$ conduction band.[29,30] The band gap of $BiFeO_3$ is determined by the energy separation between the top of O $2p$-Fe $3d$ mixed-valence band and the bottom of Fe $3d$ conduction band. On one hand, the band gap is attributed to the electron correlation between Fe $3d$ states. Such a correlation does not exist in BIT and PZT. Although the details of origin have not been clarified in this study, the electron correlation between $3d$ states may be closely related to the origin of multiferroic of $BiFeO_3$.

IV. CONCLUSION

The authors have studied the electronic structure of $BiFeO_3$ using SXES and XAS. The Fe in $BiFeO_3$ has high-spin $t_{2g}^3 e_g^2$ ground state. The conduction band consists of t_{2g} and e_g subbands of Fe $3d$ state. The valence band consists of O $2p$ state hybridized with Fe $3d$ state. The band gap corresponding to the energy separation between the top of the O $2p$-Fe $3d$ valence band and the bottom of the Fe $3d$ conduction band is 1.3 eV. The six soft x-ray Raman-scattering peaks reflect the features due to CT transition from O $2p$ valence band to Fe $3d$ conduction band. These findings are similar to the electronic structure by DFT within LSDA method that included the effect of U_{eff}.

*higuchi@rs.kagu.tus.ac.jp. Also at Department of Applied Physics, Tokyo University of Science, 1-3 Kagurazaka, Shinjuku, Tokyo 162-8601, Japan.

[1] T. Kimura, T. Goto, H. Shintani, K. Ishizaka, T. Arima, and Y. Tokura, Nature (London) **426**, 55 (2003).

[2] G. Smolenskii, V. Isupov, A. Agranovskaya, and N. Kranik, Sov. Phys. Solid State **2**, 2651 (1961).

[3] G. Smolenskii, V. Yudin, E. Sher, and Y. E. Stolypin, Sov. Phys. JETP **16**, 622 (1963).

[4] F. Kubel and H. Schmid, Acta Crystallogr., Sect. B: Struct. Sci. **46**, 698 (1990).

[5] J. R. Teague, R. Gerson, and W. J. James, Solid State Commun. **8**, 1073 (1970).

[6] D. Lebeugle, D. Colson, A. Forget, M. Viret, P. Bonville, J. F. Marucco, and S. Fusil, Phys. Rev. B **76**, 024116 (2007).

[7] J. Wang, J. B. Neaton, H. Zheng, V. Nagarajan, S. B. Ogale, B. Liu, D. Viehland, V. Vaithyanathan, D. G. Schlom, U. V. Waghmare, N. A. Spaldin, K. M. Rabe, M. Wuttig, and R. Ramesh, Science **299**, 1719 (2003).

[8] J. Li, J. Wang, M. Wuttig, R. Ramesh, N. Wang, B. Ruette, A. P. Pyatakov, A. K. Zvezdin, and D. Viehland, Appl. Phys. Lett. **84**, 5261 (2004).

[9] S. K. Singh and H. Ishiwara, Jpn. J. Appl. Phys., Part 2 **44**, L734 (2005).

[10] K. Y. Yun, D. Ricinschi, T. Kanashima, M. Noda, and M. Okuyama, Jpn. J. Appl. Phys., Part 2 **43**, L647 (2004).

[11] D. H. Kim, H. N. Lee, M. D. Biegalski, and H. M. Christen, Appl. Phys. Lett. **92**, 012911 (2008).

[12] V. R. Palkar, J. John, and R. Pinto, Appl. Phys. Lett. **80**, 1628 (2002).

[13] Y. P. Wang, L. Zhou, M. F. Zhang, X. Y. Chen, J. M. Liu, and Z. G. Liu, Appl. Phys. Lett. **84**, 1731 (2004).

[14] K. Ueda, H. Tabata, and T. Kawai, Appl. Phys. Lett. **75**, 555 (1999).

[15] M. Mahesh Kumar, A. Srinivas, and S. V. Suryanarayana, J. Appl. Phys. **87**, 855 (2000).

[16] W. Sakamoto, H. Yamazaki, A. Iwata, T. Shimura, and T. Yogo, Jpn. J. Appl. Phys., Part 1 **45**, 7315 (2006).

[17] S. Yasui, H. Uchida, H. Nakaki, K. Nishida, H. Funakubo, and S. Koda, Appl. Phys. Lett. **91**, 022906 (2007).

[18] N. Itoh, T. Shimura, W. Sakamoto, and T. Yogo, Ferroelectrics **356**, 19 (2007).

[19] J. B. Neaton, C. Ederer, U. V. Waghmare, N. A. Spaldin, and K. M. Rabe, Phys. Rev. B **71**, 014113 (2005).

[20] P. Baettig, C. Ederer, and N. A. Spaldin, Phys. Rev. B **72**, 214105 (2005).

[21] A. Kotani and S. Shin, Rev. Mod. Phys. **73**, 203 (2001).

[22] J. C. Fuggle and J. E. Inglesfield, *Unoccupied Electronic States* (Springer-Verlag, Berlin, 1991).

[23] J. Nordgren and R. Nyholm, Nucl. Instrum. Methods Phys. Res. A **246**, 242 (1986).

[24] J. Nordgren, G. Bray, S. Cramm, R. Nyholm, J. E. Rubensson, and N. Wassdahl, Rev. Sci. Instrum. **60**, 1690 (1989).

[25] J.-H. Guo, Y. Luo, A. Augustsson, J.-E. Rubensson, C. Såthe, H. Ågren, H. Siegbahn, and J. Nordgren, Phys. Rev. Lett. **89**, 137402 (2002).

[26] M. Abbate, F. M. F. de Groot, J. C. Fuggle, A. Fujimori, O. Strebel, F. Lopez, M. Domke, G. Kaindl, G. A. Sawatzky, M. Takano, Y. Takeda, H. Eisaki, and S. Uchida, Phys. Rev. B **46**, 4511 (1992).

[27] H. Wadati, D. Kobayashi, H. Kumigashira, K. Okazaki, T. Mizokawa, A. Fujimori, K. Horiba, M. Oshima, N. Hamada, M. Lippmaa, M. Kawasaki, and H. Koinuma, Phys. Rev. B **71**, 035108 (2005).

[28] H. Béa, M. Bibes, S. Fusil, K. Bouzehouane, E. Jacquet, K. Rode, P. Bencok, and A. Barthélémy, Phys. Rev. B **74**, 020101(R) (2006).

[29] T. Higuchi, M. Tanaka, K. Kudoh, T. Takeuchi, Y. Harada, S. Shin, and T. Tsukamoto, Jpn. J. Appl. Phys., Part 1 **40**, 5803 (2001).

[30] T. Higuchi, T. Tsukamoto, T. Hattori, Y. Honda, S. Yokoyama, and H. Funakubo, Jpn. J. Appl. Phys., Part 1 **44**, 6923 (2005).

[31] J. F. Ihlefeld, N. J. Podraza, Z. K. Liu, R. C. Rai, X. Xu, T. Heeg, Y. B. Chen, J. Li, R. W. Collins, J. L. Musfeldt, X. Q. Pan, J. Schubert, R. Ramesh, and D. G. Schlom, Appl. Phys. Lett. **92**, 142908 (2008).

[32] S. M. Butorin, J.-H. Guo, M. Magnuson, P. Kuiper, and J. Nordgren, Phys. Rev. B **54**, 4405 (1996).

[33] S. M. Butorin, D. C. Mancini, J.-H. Guo, N. Wassdahl, J. Nordgren, M. Nakazawa, S. Tanaka, T. Uozumi, A. Kotani, Y. Ma, K. E. Myano, B. A. Karlin, and D. K. Shuh, Phys. Rev. Lett. **77**, 574 (1996).

[34] T. Higuchi, T. Tsukamoto, M. Watanabe, M. M. Grush, T. A. Callcott, R. C. Perera, D. L. Ederer, Y. Tokura, Y. Harada, Y. Tezuka, and S. Shin, Phys. Rev. B **60**, 7711 (1999).

[35] J.-H. Guo, S. M. Butorin, N. Wassdahl, J. Nordgren, P. Berastegut, and L.-G. Johansson, Phys. Rev. B **61**, 9140 (2000).

[36] M. Magnuson, S. M. Butorin, J.-H. Guo, and J. Nordgren, Phys. Rev. B **65**, 205106 (2002).

[37] T. Higuchi, D. Baba, T. Takeuchi, T. Tsukamoto, Y. Taguchi, Y. Tokura, A. Chainani, and S. Shin, Phys. Rev. B **68**, 104420 (2003).